Supplementary Information

$[GaF(H_2O)][IO_3F]$: A Promising NLO Material Obtained by Anisotropic Polycation Substitution

Qian-Ming Huang,[a,b] Chun-Li Hu,[a] Bing-Ping Yang,*[a] Zhi Fang,[a] Yuan Lin,[a] Jin Chen,[a,b] Bing-Xuan Li,[a] and Jiang-Gao Mao*[a,b]

[a] State Key Laboratory of Structural Chemistry, Fujian Institute of Research on the Structure of Matter, Chinese Academy of Sciences, Fuzhou, 350002, P. R. China

[b] University of Chinese Academy of Sciences, Beijing, 100049, P. R. China

Table of contents

S1 METHODS

Caution: Hydrofluoric acid is highly corrosive! The appropriate personal protective equipment and standard operating procedure are essential when use it. HF should always be handled inside of a fume hood, and avoid skin and eye contact, inhalation, and ingestion.

Synthesis. Single crystals of $[GaF(H_2O)][IO_3F]$ were synthesized by a conventional hydrothermal method. All reagents were purchased from Aladdin Chemistry and without further purification. A mixture of 0.65 mmol Ga_2O_3 and 1.5 mmol HIO_3 was weighed and put into a 23 mL Teflon liner. Then, 1 mL HF aqueous solution (40%) was carefully transferred into the liner in a fume hood. The liner was promptly sealed and placed into a stainless steel autoclave and heated in an oven. The oven was heated to 230 °C in 4 hours and kept at the temperature for 67 hours and then slowly cooled to room temperature in 58 hours. Wedge-shaped prismatic crystals of $[GaF(H_2O)][IO_3F]$ were obtained in a high yield of 60-70% (based on Ga) after washing and drying.

The repeated experiments showed that the appropriate I to Ga ratio can range from 1.0 to 1.5, and HIO_3 can be replaced by I_2O_5 and H_5IO_6. The amount of hydrofluoric acid is very critical and insufficient or excessive HF will lead to the formation of $Ga(IO_3)_3$. Besides, high reaction temperature (equal to or above 230 °C) facilitates the synthesis of the target products. It is worth noting that the synthesis condition of $[GaF(H_2O)][IO_3F]$ is very simialr to that of $CsIO_2F_2$.[1]

Single crystal structure determination. Some $[GaF(H_2O)][IO_3F]$ crystals were cut into appropriate sizes and a high-quality crystal was selected, mounted on a glass fiber, and inserted into the goniometer head for single-crystal structural determination. The diffraction data were collected on a Rigaku Oxford Diffraction SuperNova CCD diffractometer with Mo Kα radiation (λ = 0.71073 Å) at 294.86 K. Cell refinement and data reduction were performed using CrysAlisPro. Numerical absorption correction based on Gaussian integration over a multifaceted crystal model and empirical absorption correction using spherical harmonics were implemented in the

SCALE3 ABSPACK scaling algorithm.[2] The structure was determined by the direct method and refined by full-matrix least-squares fitting on F^2 using SHELXL.[3, 4] All of the atoms were refined with anisotropic thermal parameters. The structure was checked for missing symmetry elements using PLATON, and none was suggested.[5] The flack parameter was refined to 0.01(5) for the title compound, indicating the correctness of the absolute structure.[6] Crystallographic data and structural refinements of the compound are listed in Table S2, and some selected bond lengths and angles are listed in Table S4 and S5.

Powder X-ray Diffraction (PXRD). PXRD analysis was performed on a Rigaku MiniFlex600 diffractometer equipped with graphite monochromator Cu Kα radiation (λ = 1.54186 Å) in the 2θ range of 10−60° with a scanning step width of 0.02°.

Energy-dispersive X-ray Spectroscope (EDS). Microprobe elemental analysis was measured using a field-emission scanning electron microscope (FESEM, JSM6700F) equipped with an energy-dispersive X-ray spectroscope (EDS, Oxford INCA).

Spectroscopic Measurements. IR spectrum was recorded on a Magna 750 FT−IR spectrometer in the form of KBr pellet in the range of 4000−400 cm^{-1}. UV−vis− NIR diffuse reflection spectrum in the range of 200−2000 nm was recorded on a PerkinElmer Lambda 950 UV−vis−NIR spectrophotometer with $BaSO_4$ powder plate used as a 100% reflectance reference. Absorption data were calculated from the diffuse-reflectance data using the Kubelka-Munk function: $\alpha/S = (1-R)^2/2R$, where α is the absorption coefficient, S is the scattering coefficient.[7] The extrapolation of the absorption edge to the baseline in the α/S versus Energy diagram gives the band gap value.

Thermal Analyses. Thermogravimetric Analysis (TGA) and differential scanning calorimetry (DSC) were performed on a NETZCH STA 449F3 thermal analyzer instrument. Powder samples were put in an Al_2O_3 crucible with an empty crucible used as a reference and heated from 20 to 1000 °C at a rate of 15 °C min^{-1} under a nitrogen atmosphere.

Thermogravimetric Spectrometry (TG-MS) Analyses. TG-MS analyses were

carried out on pre-weighted samples in a nitrogen stream using a Rigaku (thermo plus EV2/ thermo mass photo) apparatus.

X-ray Photoelectron Spectroscopy (XPS). XPS characterization was accomplished using an ESCALAB 250Xi instrument with an Al Kα radiation exciting source and was performed on the pure and uniform powder sample.

Solid-State Nuclear Magnetic Resonance (NMR) Spectrum. ^{19}F MAS Nuclear magnetic resonance (^{19}F NMR) spectrum was collected on an AVANCE III 500M Bruker spectrometer with a spinning frequency of 96340.8 Hz.

Elemental analysis (EA). Elemental analysis was carried out using an ELEMENTAR VARIO EL CUBE elemental analyzer. The sample was burned in the elemental analyzer, and the final gaseous products H_2O were separated on a gas chromatograph and quantified.

Second-Harmonic Generation (SHG) Measurements. Powder SHG of sieved samples was measured using a modified method of Kurtz and Perry[8] with laser irradiation of λ = 1064 nm generated by a Q-switched Nd:YAG solid-state laser. Pure polycrystalline $[GaF(H_2O)][IO_3F]$ samples were ground and sieved into eight different particle size ranges (0–25, 25–45, 45–53, 53–75, 75–105, 105–150, 150–210, >210 μm). Sieved KH_2PO_4 (KDP) samples of the same particle size ranges were measured as references. Oscilloscope traces of SHG signals of $[GaF(H_2O)][IO_3F]$ and KDP samples in the particle-size range of 150–210 μm were recorded.

Laser-induced Damage Threshold (LDT) Measurements. LDT of $[GaF(H_2O)][IO_3F]$ was measured on the crystalline samples together with AGS samples of the same size as a reference using a Q-switched pulsed laser (1064 nm, 10 ns, 1Hz). The area of the laser spot focused on the samples is 1.5315 mm^2. The laser emission energy was gradually increased until the color of the samples turned black, and the laser energy value at its height was considered as the LDT of the samples. LDT measurement using polycrystalline samples is feasible because each crystallite has a diameter much larger than the wavelength of the incident laser and behaves as a macroscopic bulk material with the similar multiphoton absorption (the main process

for LDT as the laser pulse width is smaller than 50 *p*s).[9]

Computational Methods. The calculations of electronic and optical properties were performed with the CASTEP code using the plane-wave pseudopotential density functional theory (DFT).[10, 11] Generalized gradient approximation (GGA) Perdew−Burke−Ernzerhof (PBE) was chosen as the exchange-correlation functional.[12] The core−electron interactions were represented by the norm-conserving pseudopotential.[13] Ga $4s^2 4p^4$, I $5s^2 5p^5$, O $2s^2 2p^4$, F $2s^2 2p^5$ orbital electrons were set as the valence electrons. A cutoff energy of 300 eV was utilized for determination of the number of plane-wave basis sets. The Monkhorst−Pack *k*-point sampling was 1 × 3 × 4 for numerical integration over the Brillouin zone. More than 240 empty bands were used during the optical property calculations.

Geometry optimization was applied to the single-crystal structure of $[GaF(H_2O)][IO_3F]$ with disordered I atom because optical property theoretical calculations are unfeasible for a disordered structure. The minor component I1B with the occupancy of 0.14 was removed from the structure and the occupancy parameter of the major component I1A with the primitive occupancy of 0.86 was set as 1.0. Geometry optimization was carried out with the CASTEP Geometry Optimization task using the default BFGS geometry optimization method. This is done by performing an iterative process in which the coordinates of the atoms are adjusted so that the total energy of the structure is minimized. After optimization, the lowest energy structure that closely resembles the real structure was obtained and the crystal symmetry of the disorder-free $[GaF(H_2O)][IO_3F]$ was not changed compared to its original structure.

The second-order NLO properties of the material were calculated implementing the length-gauge formalism in the independent-particle approximation. According to the latest research,[14] static SHG susceptibility can be written as $\chi^{\alpha\beta\gamma} = \chi^{\alpha\beta\gamma}(\mathrm{VE}) + \chi^{\alpha\beta\gamma}(\mathrm{VH})$, Where $\chi^{\alpha\beta\gamma}(\mathrm{VE})$ is contributed by virtual-electron processes and $\chi^{\alpha\beta\gamma}(\mathrm{VH})$ is contributed by virtual-hole processes. The formulae of $\chi^{\alpha\beta\gamma}(\mathrm{VE})$ and $\chi^{\alpha\beta\gamma}(\mathrm{VH})$ are given in Chen's paper.[15]

S2 Determining the O and F atoms of the crystallographic structure.

XPS analyses revealed that the molar ratio of Ga : I : O : F is 1 : 1 : 4 : 2. The solid-state ^{19}F NMR spectrum displays two peaks with characteristic F chemical shift values and that these correspond to the two different F environments that can exist. EA result shows that the percentage of H in the original sample is 0.65%, corresponding to two H atoms of the molecular formula. The TG-MS results manifest the existence of F atoms and one coordinating H_2O, and the absence of OH groups in the molecule. The IR spectrum also verifies the presence of H_2O. Therefore, the empirical formula is $GaIO_3F_2(H_2O)$, combined with the bond lengths, bond valence sum (BVS) calculations (Table S3), and the atomic displacement parameters on the basis of the single-crystal X-ray crystallographic data, O and F atoms of the structure were determined. There is no doubt that O(1) and O(2) atoms with typical I−O bond lengths (about 1.8 Å) are in the right position. Terminal O(4) with the Ga−O bond valence of 0.54 should bond to two H atoms, which constitutes the coordinating H_2O. BVS of the bridging F(2) is 0.88, verifying the correctness of the F atom. The most complicated thing is to distinguish O(3) and F(1) atoms that are bonded to the disordered I. A disordered O/F atom model was considered; however, when the common occupancies for disordered components are refined, the final value for the occupancy parameter of O(3) is 0.732, and the occupancy parameter of F(1) is 1.09 and negative occupancy for the O component is observed. Thus, all of the O and F atoms of the structure were determined and the revised formula is $[GaF(H_2O)][IO_3F]$.

Table S1. Classification of the reported fluorine iodates.

Structure types	Compounds	Space group	Fluorine-containing units	SHG effect	Band gap	Ref
Iodate fluorides	$Bi(IO_3)F_2$	*C*2	$[BiF_2]^+$	11.5 × KDP	3.97 eV	16
	$Bi_3OF_3(IO_3)_4$	$P6_3mc$	$[BiO_7F_2]^{13-}$	6.0 × KDP	3.70 eV	17
	$KBi_2(IO_3)_2F_5$	$P2_1$	$[BiF_5]^{2-}$; $[BiO_2F_4]^{5-}$	12.0 × KDP	3.75 eV	18
	$RbBi_2(IO_3)_2F_5$	$P2_1$	$[BiF_5]^{2-}$; $[BiO_2F_4]^{5-}$	9.5 × KDP	3.78 eV	18
	$CsBi_2(IO_3)_2F_5$	$P2_1$	$[BiF_5]^{2-}$; $[BiO_2F_4]^{5-}$	7.5 × KDP	3.84 eV	18
	$NH_4Bi_2(IO_3)_2F_5$	$P2_1$	$[BiO_2F_5]^{6-}$; $[BiO_4F_4]^{9-}$	9.2 × KDP	3.88 eV	19
	β-$Ba[VFO_2(IO_3)_2]$	$P2_12_12_1$	$[VO_4F]^{4-}$	1.5 ×KDP	2.69 eV	20
	α-$Ba_2[VO_2F_2(IO_3)_2]IO_3$	$Pna2_1$	$[VO_4F_2]^{5-}$	9.0 × KDP	2.55 eV	20
	β-$Ba_2[VO_2F_2(IO_3)_2]IO_3$	$P2_1$	$[VO_4F_2]^{5-}$	9.0 ×KDP	2.59 eV	20
	α-$Ba_2[GaF_4(IO_3)_2]IO_3$	$Pna2_1$	$[GaO_2F_4]^{5-}$	6.0 × KDP	4.61 eV	21
	β-$Ba_2[GaF_4(IO_3)_2]IO_3$	$P2_1$	$[GaO_2F_4]^{5-}$	6.0 × KDP	4.35 eV	21
	$K_5(W_3O_9F_4)(IO_3)$	*Pm*	$[W_3O_{12}F_4]^{10-}$	11.0 × KDP	3.83 eV	22
	$CsVO_2F(IO_3)$	$Pna2_1$	$[VO_5F]^{6-}$	1.1 × KTP	2.39 eV	23
	$Ce(IO_3)_2F_2·H_2O$	*Ima*2	$[CeO_5F_4]^{10-}$	3.0 × KDP	2.60 eV	24
	$Sn(IO_3)_2F_2$	$P2_1$	$[SnO_4F_2]^{6-}$	3.0 × KDP	4.08 eV	25
	$Y(IO_3)_2F$	$P6_5$	$[YO_6F_2]^{-11}$	2.0 × KDP	3.91 eV	26
	$CdIO_3F$	$P2_12_12_1$	$[CdO_5F_2]^{10-}$	6.2 × KDP	4.22 eV	27
Fluoroiodates	KIO_2F_2	$Pca2_1$	$[IO_2F_2]^-$	N/A	N/A	28
	$RbIO_2F_2$	$Pca2_1$	$[IO_2F_2]^-$	4.0 × KDP	4.20 eV	29
	$CsIO_2F_2$	$Pca2_1$	$[IO_2F_2]^-$	3.0 × KDP	4.50 eV	1
This work	**$[GaF(H_2O)][IO_3F]$**	***Pca*2$_1$**	**$[GaF(H_2O)]^{2+}$; $[IO_3F]^{2-}$**	**10 × KDP**	**4.34 eV**	

Table S2. Crystallographic data and structure refinement parameters for $[GaF(H_2O)][IO_3F]$.

Formula	$[GaF(H_2O)][IO_3F]$
Formula weight	300.64
Temperature/K	294.86(10)
Crystal system	orthorhombic
Space group	$Pca2_1$
a/Å	13.9538(16)
b/Å	6.9261(9)
c/Å	4.7629(6)
α/°	90
β/°	90
γ/°	90
Volume/Å^3	460.31(10)
Z	4
ρ_{calc}g/cm^3	4.338
μ/mm^{-1}	12.656
F(000)	544.0
Radiation	MoKα (λ = 0.71073)
Independent reflections	1091 [R_{int} = 0.0406, R_{sigma} = 0.0488]
Goodness-of-fit on F^2	1.058
Final R indexes [I>=2σ (I)]	R_1 = 0.0369, wR_2 = 0.0804
Final R indexes [all data]	R_1 = 0.0388, wR_2 = 0.0814
Flack parameter	0.00(5)

[a] $R_1 = \Sigma||F_o|-|F_c||/\Sigma|F_o|$; and $wR_2 = \{\Sigma[w(F_o^2-F_c^2)^2]/\Sigma[w(F_o^2)^2]\}^{1/2}$

Table S3. Fractional atomic coordinates ($\times 10^4$), equivalent isotropic displacement parameters ($Å^2 \times 10^3$) and bond valence sums (BVS) for $[GaF(H_2O)][IO_3F]$. U_{eq} is defined as 1/3 of the trace of the orthogonalised U_{ij} tensor.

Atom	*x*	*y*	*z*	U(eq)	BVS
Ga1	4286.8(7)	6348.3(14)	4711(3)	9.1(3)	3.15
F2	5268(4)	5761(8)	2026(13)	13.7(13)	0.88
F1	6185(4)	11762(8)	7300(20)	16.5(18)	0.79
O4	3262(5)	6861(9)	7420(20)	15.0(16)	2.54
O1	6889(5)	8465(10)	4314(17)	15.5(16)	1.8
O3	6561(4)	5500(9)	7945(19)	11.1(15)	1.9
O2	5080(5)	8152(10)	6601(17)	13.8(16)	2.24
I1A	6343.0(13)	8138(9)	7654(3)	9.1(6)	4.97
I1B	6259(7)	8910(50)	7580(30)	9(3)	

Table S4. Selected bond lengths for $[GaF(H_2O)][IO_3F]$.

Bond	Bond length/Å	Bond	Bond length/Å
Ga1-F2	1.917(6)	O1-I1A	1.778(8)
Ga1-F2[1]	1.933(6)	O2-I1A	1.832(7)
Ga1-F1[2]	1.860(8)	O3-I1A	1.858(9)
Ga1-O4	1.958(8)	F1-I1B	1.98(4)
Ga1-O3[3]	1.936(7)	O1-I1B	1.815(15)
Ga1-O2	1.896(7)	O2-I1B	1.790(10)
F1-I1A	2.5254(3)	O3-I1B	2.41(4)

Symmetry transformations: [1]1-X,1-Y,1/2+Z; [2]1-X,2-Y,-1/2+Z; [3]1-X,1-Y,-1/2+Z; [4]1-X,2-Y,1/2+Z.

Table S5. Selected bond angles for $[GaF(H_2O)][IO_3F]$.

Angle	Degree	Angle	Degree
F2-Ga1-F2[1]	89.46(12)	O2-Ga1-F2	92.3(3)
F2-Ga1-O4	178.0(3)	O2-Ga1-O4	89.7(3)
F2[1]-Ga1-O4	89.8(3)	O2-Ga1-O3[2]	177.2(4)
F2[1]-Ga1-O3[2]	86.8(3)	O1-I1A-O3	97.0(4)
F2-Ga1-O3[2]	90.4(3)	O1-I1A-O2	99.6(4)
F1[3]-Ga1-F2	89.5(3)	O2-I1A-O3	100.6(3)
F1[3]-Ga1-F2[1]	175.6(3)	F1-I1B-O3	172.9(4)
F1[3]-Ga1-O4	91.1(4)	O1-I1B-F1	98.0(13)
F1[3]-Ga1-O3[2]	88.9(3)	O1-I1B-O3	79.0(12)
F1[3]-Ga1-O2	92.0(3)	O2-I1B-F1	103.2(14)
O3[2]-Ga1-O4	87.7(3)	O2-I1B-O1	99.8(7)
O2-Ga1-F2[1]	92.3(3)	O2-I1B-O3	83.7(12)

Symmetry transformations: [1]1-X,1-Y,1/2+Z; [2]1-X,1-Y,-1/2+Z; [3]1-X,2-Y,-1/2+Z; [4]1-X,2-Y,1/2+Z.

Table S6. Calculated dipole moments of IO_3F and GaO_3F_3 units, and net dipole moment of a unit cell for $[GaF(H_2O)][IO_3F]$.

$[GaF(H_2O)][IO_3F]$ (Z = 4)				
Species	Dipole moment (D = Debye)			
	x(a)	y(b)	z(c)	total magnitude
$I(1)O_3F$	3.477	-1.849	-10.548	11.260
$I(2)O_3F$	-3.477	-1.849	-10.548	11.260
$I(3)O_3F$	3.477	1.849	-10.548	11.260
$I(4)O_3F$	-3.477	1.849	-10.548	11.260
$Ga(1)O_3F_3$	-0.991	0.394	0.094	0.180
$Ga(2)O_3F_3$	0.991	0.394	0.094	0.180
$Ga(3)O_3F_3$	-0.991	-0.394	0.094	0.179
$Ga(4)O_3F_3$	0.991	-0.394	0.094	0.181
Unit cell	0	0	-41.82	41.82
The dipole moment density ($D/Å^3$)			0.0908	

Table S7. Comparisons of dipole moments for $[GaF(H_2O)][IO_3F]$ and $CsIO_2F_2$.

Compound	Dipole moment within a unit cell (D)				Volume/ $Å^3$	The dipole moment density ($D/Å^3$)
	x(a)	y(b)	z(c)	total		
$[GaF(H_2O)][IO_3F]$	0	0	-41.82	41.82	460.31	0.0908
$CsIO_2F_2$	-0.006	-0.001	33.769	33.769	496.60	0.0680

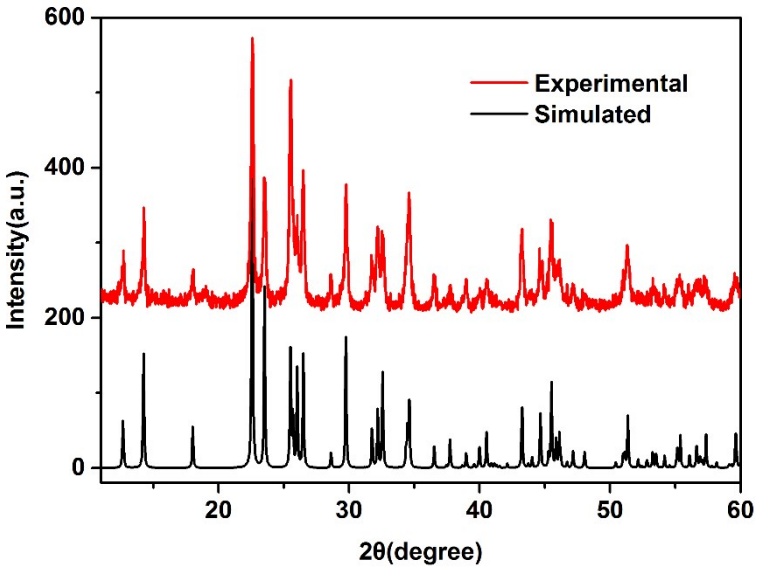

Figure S1. Simulated and measured PXRD patterns of [GaF(H_2O)][IO_3F].

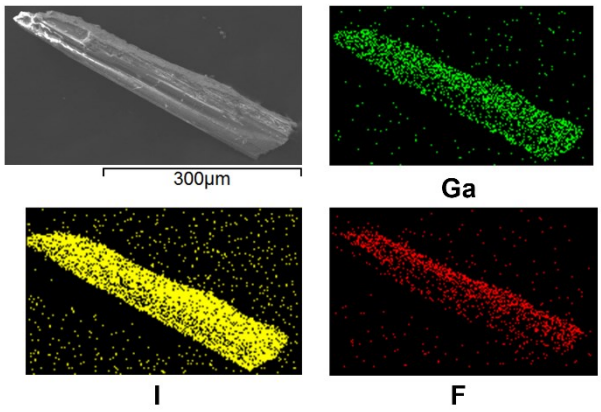

Figure S2. SEM image of [GaF(H_2O)][IO_3F] and its elemental distribution maps.

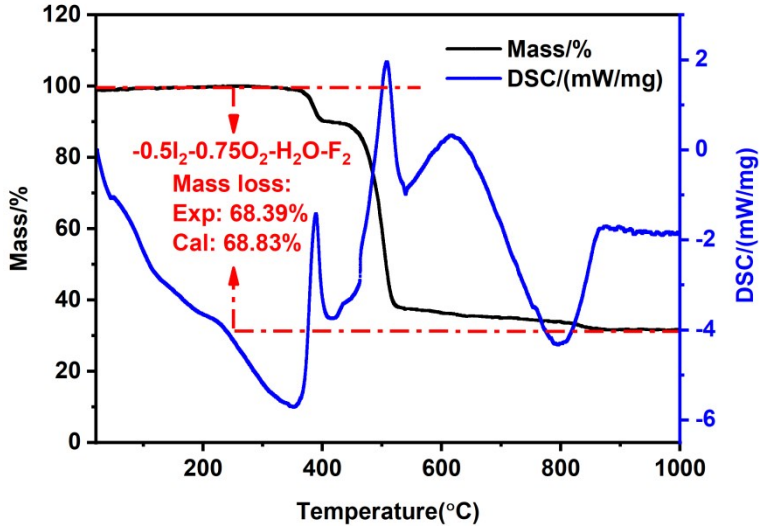

Figure S3. TGA and DSC curves of $[GaF(H_2O)][IO_3F]$ under N_2 atmosphere.

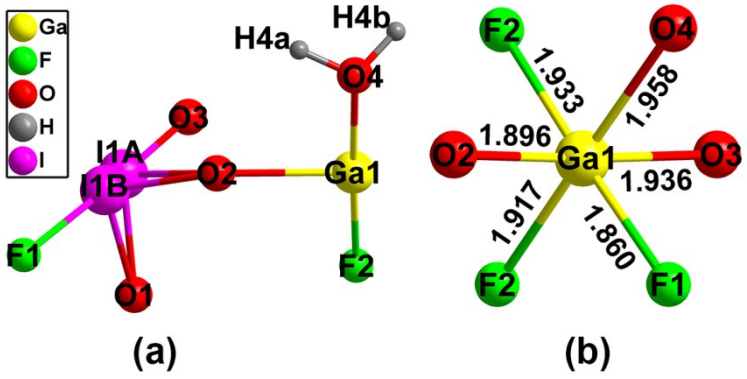

Figure S4. View of the (a) asymmetric unit (b) GaO_3F_3 octahedron.

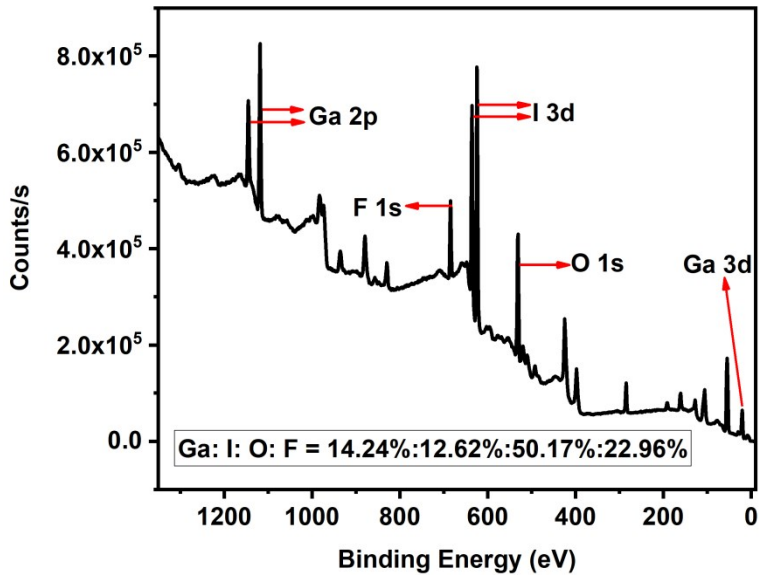

Figure S5. XPS spectrum of $[GaF(H_2O)][IO_3F]$.

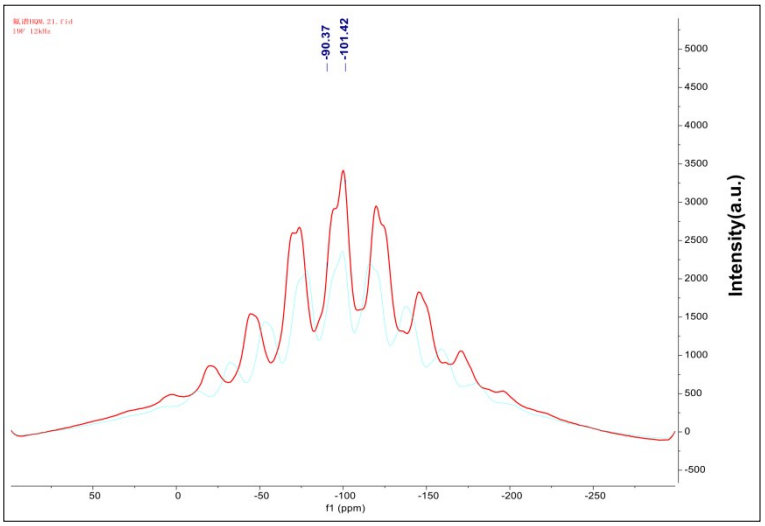

Figure S6. ^{19}F MAS NMR spectrum of $[GaF(H_2O)][IO_3F]$.

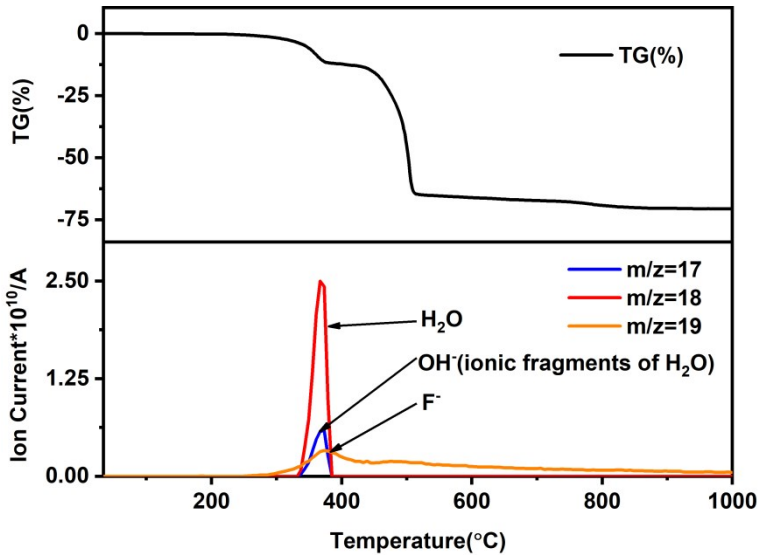

Figure S7. TG-MS curves of $[GaF(H_2O)][IO_3F]$.

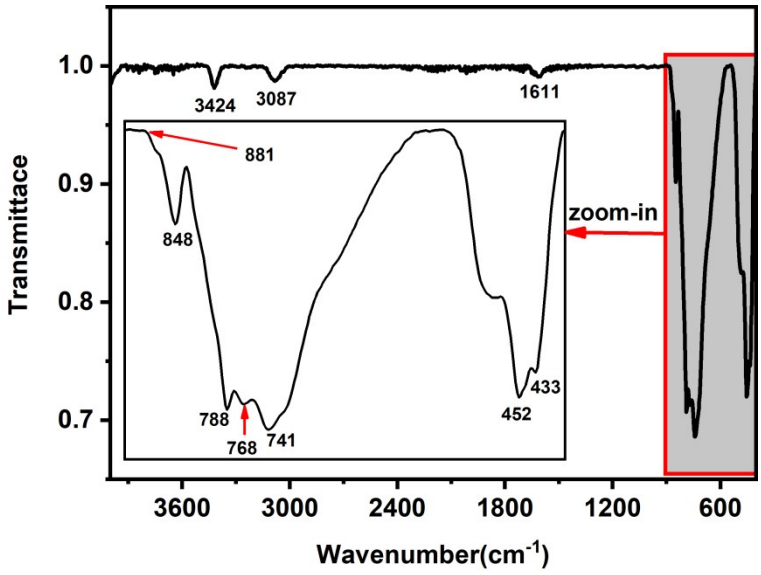

Figure S8. IR spectrum of $[GaF(H_2O)][IO_3F]$, inset: zoomed-in view of IR bands.

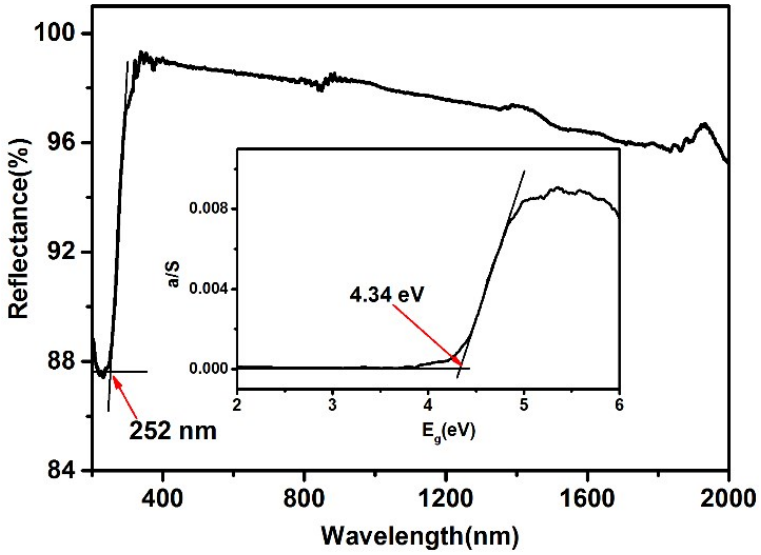

Figure S9. UV-vis-NIR spectrum of [GaF(H_2O)][IO_3F].

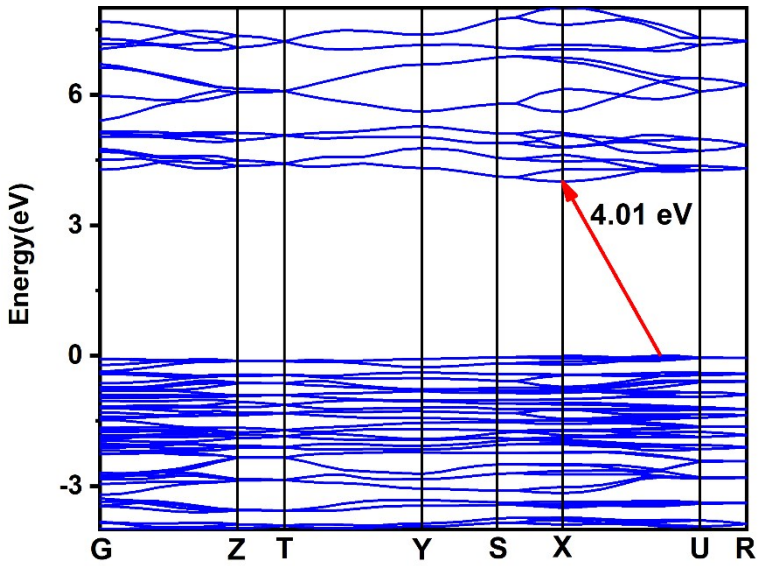

Figure S10. Calculated band structure of [GaF(H_2O)][IO_3F].

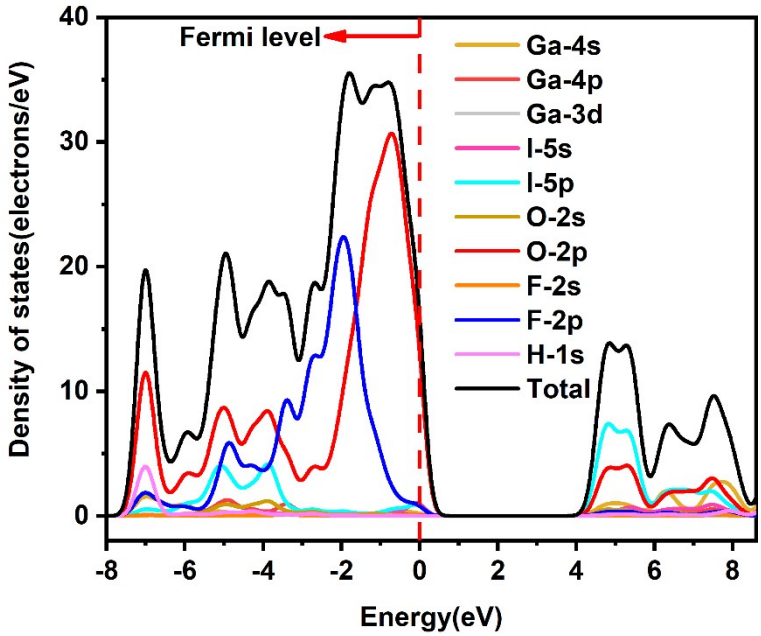

Figure S11. Partial and total density of states for $[GaF(H_2O)][IO_3F]$.

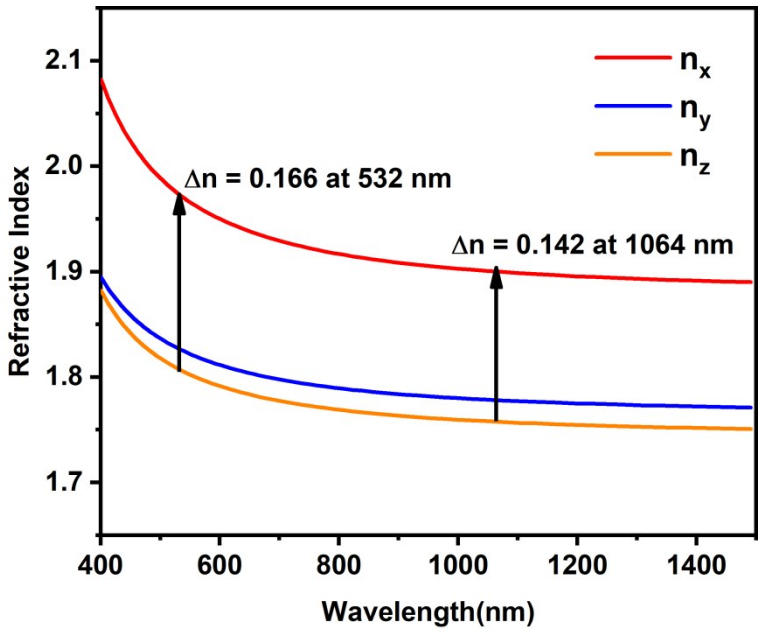

Figure S12. Calculated frequency-dependent refractive indices of $[GaF(H_2O)][IO_3F]$.

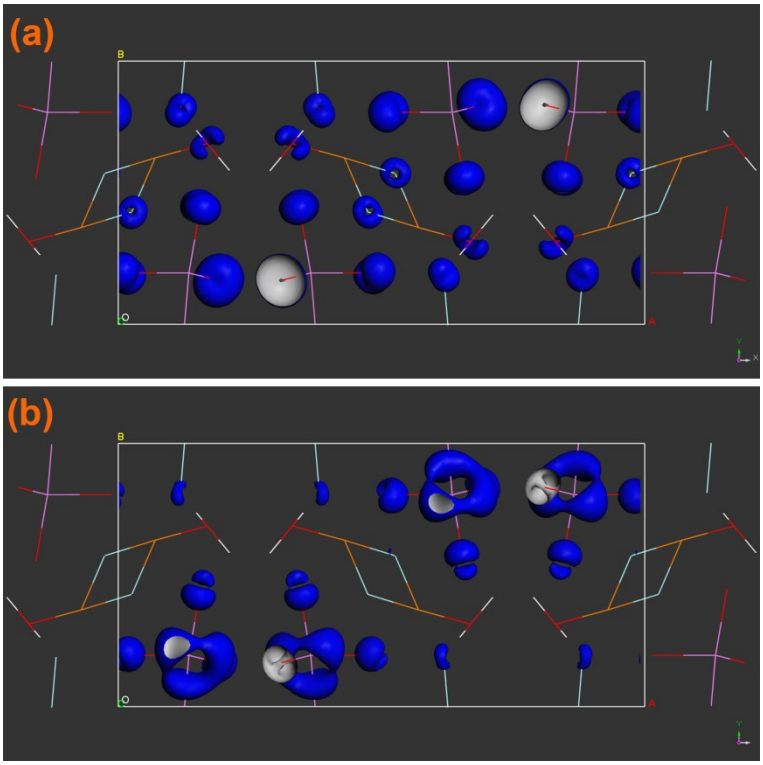

Figure S13. SHG density of d_{32} in the (a) CB and (b) VB for [GaF(H_2O)][IO_3F].

Reference:

1 M. Zhang, C. Hu, T. Abudouwufu, Z. Yang and S. Pan, *Chem. Mater.*, 2018, **30**, 1136-1145.

2 R. H. Blessing, *Acta Crystallogr., Sect. A: Found. Crystallogr.*, 1995, **51**, 33-38.

3 G. M. Sheldrick, *Acta Crystallogr A Found Adv*, 2015, **71**, 3-8.

4 G. M. Sheldrick, *Acta Crystallogr C Struct Chem*, 2015, **71**, 3-8.

5 A. L. Spek, *J. Appl. Crystallogr.*, 2003, **36**, 7-13.

6 H. D. Flack, *Acta Crystallogr., Sect. A: Found. Crystallogr.*, 1983, **39**, 876-881.

7 Kubelka and Munk, *Zeit. Für Tekn. Physik*, 1931, **12**, 593.

8 S. K. Kurtz and T. T. Perry, *J. Appl. Phys.*, 1968, **39**, 3798-3813.

9 S. P. Guo, X. Cheng, Z. D. Sun, Y. Chi, B. W. Liu, X. M. Jiang, S. F. Li, H. G. Xue, S. Deng, V. Duppel, J. Kohler and G. C. Guo, *Angew. Chem. Int. Ed.*, 2019, **58**, 8087-8091.

10 V. Milman, B. Winkler, J. A. White, C. J. Pickard, M. C. Payne, E. V. Akhmatskaya and R. H. Nobes, *Int. J. Quantum Chem.*, 2000, **77**, 895-910.

11 M. D. Segall, P. J. D. Lindan, M. J. Probert, C. J. Pickard, P. J. Hasnip, S. J. Clark and M. C. Payne, *J Phys-Condens Mat*, 2002, **14**, 2717-2744.

12 J. P. Perdew, K. Burke and M. Ernzerhof, *Phys. Rev. Lett.*, 1996, **77**, 3865-3868.

13 J. S. Lin, A. Qteish, M. C. Payne and V. Heine, *Phys Rev B*, 1993, **47**, 4174-4180.

14 B. Zhang, M.-H. Lee, Z. Yang, Q. Jing, S. Pan, M. Zhang, H. Wu, X. Su and C.-S. Li, *Appl. Phys. Lett.*, 2015, **106**, 031906-031905.

15 J. Lin, M. H. Lee, Z. P. Liu, C. T. Chen and C. J. Pickard, *Phys Rev B*, 1999, **60**, 13380-13389.

16 F. F. Mao, C. L. Hu, X. Xu, D. Yan, B. P. Yang and J. G. Mao, *Angew. Chem. Int. Ed.*, 2017, **56**, 2151-2155.

17 M. Zhang, X. Su, M. Mutailipu, Z. Yang and S. Pan, *Chem. Mater.*, 2017, **29**, 945-949.

18 H. Liu, Q. Wu, X. Jiang, Z. Lin, X. Meng, X. Chen and J. Qin, *Angew. Chem. Int. Ed.*, 2017, **56**, 9492-9496.

19 H. Fan, C. Lin, K. Chen, G. Peng, B. Li, G. Zhang, X. Long and N. Ye, *Angew. Chem. Int. Ed.*, 2020, **59**, 5268-5272.

20 H. Yu, M. L. Nisbet and K. R. Poeppelmeier, *J. Am. Chem. Soc.*, 2018, **140**, 8868-8876.

21 J. Chen, C. L. Hu, F. F. Mao, J. H. Feng and J. G. Mao, *Angew. Chem. Int. Ed.*, 2019, **58**, 2098-2102.

22 C. Wu, L. Lin, X. Jiang, Z. Lin, Z. Huang, M. G. Humphrey, P. S. Halasyamani and C. Zhang, *Chem. Mater.*, 2019, **31**, 10100-10108.

23 J. Chen, C. L. Hu, X. H. Zhang, B. X. Li, B. P. Yang and J. G. Mao, *Angew. Chem. Int. Ed.*, 2020, **59**, 5381-5384.

24 T. Abudouwufu, M. Zhang, S. Cheng, Z. Yang and S. Pan, *Chemistry*, 2019, **25**, 1221-1226.

25 M. Luo, F. Liang, X. Hao, D. Lin, B. Li, Z. Lin and N. Ye, *Chem. Mater.*, 2020, **32**, 2615-2620.

26 G. Peng, Y. Yang, T. Yan, D. Zhao, B. Li, G. Zhang, Z. Lin and N. Ye, *Chemical Science*, 2020, DOI: 10.1039/d0sc02789h.

27 L. Cao, M. Luo, C. Lin, Y. Zhou, D. Zhao, T. Yan and N. Ye, *Chem. Commun.*, 2020, **56**, 10734-10737.

28 S. C. Abrahams and J. L. Bernstein, *J. Chem. Phys.*, 1976, **64**, 3254-3260.

29 Q. Wu, H. Liu, F. Jiang, L. Kang, L. Yang, Z. Lin, Z. Hu, X. Chen, X. Meng and J. Qin, *Chem. Mater.*, 2016, **28**, 1413-1418.